

Fifth-Order Weighted Power-ENO Schemes for Hamilton-Jacobi Equations

Susana Serna,¹ and Jianliang Qian²

Received September 30, 2004; accepted (in revised form) May 19, 2005

We design a class of Weighted Power-ENO (Essentially Non-Oscillatory) schemes to approximate the viscosity solutions of Hamilton-Jacobi (HJ) equations. The essential idea of the Power-ENO scheme is to use a class of extended limiters to replace the minmod type limiters in the classical third-order ENO schemes so as to improve resolution near kinks where the solution has discontinuous gradients. Then a weighting strategy based on appropriate smoothness indicators lifts the scheme to be fifth-order accurate. In particular, numerical examples indicate that the Weighted Power₃ENO5 works for general HJ equations while the Weighted Power_∞ENO5 works for non-linear convex HJ equations. Numerical experiments also demonstrate the accuracy and the robustness of the new schemes.

KEY WORDS: Hamilton-Jacobi; ENO; Weighted Power-ENO; level set; monotone schemes.

1. INTRODUCTION

We consider the initial value problem for the Hamilton-Jacobi equation

$$\phi_t + H(x, \phi, \nabla\phi) = 0, \quad \phi(x, 0) = \phi_0(x), \quad x \in R^d, \quad t > 0, \quad (1.1)$$

where H is a non-decreasing function of ϕ .

Such Hamilton-Jacobi (HJ) equations appear in many applications, for example, geometrical optics, optimal control, differential games, material sciences and calculus of variations. Therefore, it is essential to develop efficient, high-order accurate numerical methods to solve these equations.

¹ Departamento de Matematica Aplicada, University of Valencia, Valencia, Spain. E-mail: susana.serna@uv.es

² Department of Mathematics, UCLA, Los Angeles, CA 90095-1555, USA. E-mail: qian@math.ucla.edu

Theoretically, the generalized weak solution, the so-called viscosity solution, exists, is unique and depends on the initial data continuously [8]. Computationally, such viscosity solutions can be approximated by monotone schemes [5, 9, 24]. Since monotone schemes are at most first order accurate, a lot of efforts are devoted to designing efficient, highly accurate numerical schemes for such equations (see [1–4, 6, 10, 14, 17, 19–21, 26] and references therein). In this paper, we design a class of new schemes for HJ equations based on the Weighted Power-ENO (“Essentially Non-Oscillatory”) reconstruction, which is formally fifth-order accurate.

In general, the high-order schemes in the ENO family for HJ equations consist of three ingredients: a monotone numerical Hamiltonian, a high-order ENO type reconstruction and a high-order strong stability preserving Runge-Kutta (SSP-RK) time stepping procedure [14, 20]; these are so-called ENO schemes. Because monotone numerical Hamiltonians [20] and high-order SSP-RK time discretization methods [11, 25] are well developed, the main issue is how to build high-order ENO type reconstructions. The ENO schemes were originally designed for hyperbolic conservation laws by Harten *et al.* [13]. Later the schemes were adapted to solve HJ equations by Osher and Sethian [19] and Osher and Shu [20]. Liu *et al.* [18] proposed the Weighted ENO schemes to overcome some shortcomings of ENO schemes, such as poor parallelizability. Afterwards, Jiang and Shu [15] realized that the weighting strategy may yield other advantages besides parallelizability, such as higher order accuracy and stability. Moreover, Jiang and Peng [14] extended such strategy to design WENO schemes for HJ equations. Since then, such a weighting strategy has been used successfully in designing high-order schemes for HJ equations: Weighted central ENO schemes [3], Hermite WENO schemes [21], high-order WENO schemes on unstructured meshes [26] which in turn used the numerical Hamiltonian proposed in [1]. In this work we propose yet another class of weighted schemes for HJ equations, the so-called Weighted Power-ENO schemes.

The Weighted Power-ENO schemes were originally developed by Serna and Marquina [22] for hyperbolic conservation laws. The essential idea of the Power-ENO reconstruction is to apply a class of extended limiters to second-order differences in the classical third-order ENO reconstruction, so that the reconstruction is able to retain more information of the fine scales of the solution and improve resolution near discontinuities of the solution. A weighting strategy based on appropriate smoothness indicators [15] is then used to improve the reconstruction to be fifth-order accurate; this is the so-called Weighted Power-ENO reconstruction. Here we adapt such Weighted Power-ENO reconstruction to HJ equations; the resulting scheme is the so-called Weighted Power₃ENO₅ scheme

(WPower₃ENO5 in the sequel.) In addition, we are able to design a new Weighted Power-ENO reconstruction specifically for HJ equations with convex Hamiltonians, and it is based on the so-called arithmetic mean type limiter; the resulting scheme is the so-called Weighted Power_∞ENO5 scheme (WPower_∞ENO5 in the sequel.) In comparison to the standard fifth-order WENO scheme, the resulting schemes enjoy similar overhead and have much better capability of resolving viscosity solutions near kinks where the solution has discontinuous gradients as illustrated in the numerical examples.

The paper is organized as follows. In Sec. 2, we derive the Weighted Power-ENO reconstructions and present some standard monotone numerical Hamiltonians; together with a SSP-RK time stepping method [11, 23, 25], the above two ingredients complete the construction of new Weighted Power-ENO type schemes. In Sec. 3, we give extensive numerical examples to demonstrate the accuracy and the resolution capability of the new schemes. Concluding remarks are provided in Sec. 4.

2. NEW NUMERICAL SCHEMES

2.1. Weighted Power-ENO Reconstructions

The classical third-order ENO reconstruction on a uniform mesh uses an adaptive procedure to choose one three-point stencil among three such candidates. Since such a three-point stencil uniquely determines a parabola, the ENO strategy boils down to using only one among three available parabolas.

The Power-ENO is designed by incorporating a class of new limiters into the classical third-order ENO reconstruction. Namely, the minmod-type limiter in the classical ENO reconstruction is replaced by a class of weaker limiters, the so-called power_{*p*} limiters; then the new limiters are applied to neighboring second-order differences so that more information of fine scales is retained.

As a consequence, a carefully designed convex combination of the three candidate parabolas gives rise to the Weighted Power-ENO reconstruction; the resulting Weighted Power-ENO scheme was applied to the hyperbolic conservation laws [22] and demonstrated to have better capability to resolve discontinuities of solutions.

Encouraged by the success in hyperbolic conservation laws, we adapt the Weighted Power-ENO reconstruction to tackle HJ equations so as to improve the resolution near kinks where the gradient of the solution is discontinuous. We start with the power_{*p*} limiters.

Let $x > 0$ and $y > 0$ be positive numbers. For a natural number p , the power- p mean, $\text{power}_p(x, y)$, was defined in [22]:

$$\text{power}_p(x, y) = \frac{(x+y)}{2} \left(1 - \left| \frac{x-y}{x+y} \right|^p \right). \quad (2.1)$$

It is easy to verify that the following inequalities hold for any $x > 0$ and $y > 0$:

$$\min(x, y) \leq \text{power}_p(x, y) \leq \text{power}_q(x, y) \leq \frac{x+y}{2}$$

when $0 < p < q$. Moreover,

$$\lim_{p \rightarrow \infty} \text{power}_p(x, y) = \frac{x+y}{2} := \text{power}_\infty(x, y), \quad (2.2)$$

which is an arithmetic mean.

Given point values $\phi(x_j)$, $j = 0, 1, 2, \dots$, of a (possibly piecewise smooth) function at equally spaced nodes x_j , where $x_{j+1} = x_j + \Delta x$, we construct higher order approximations to first-order forward and backward divided differences at a generic node x_j by using the power- p limiters. To do that, we first compute forward divided differences,

$$z_{j+\frac{1}{2}} = \frac{\Delta_+ \phi_j}{\Delta x} = \frac{\phi_{j+1} - \phi_j}{\Delta x} \quad (2.3)$$

from discrete point values, $\phi = \phi(x_j)$, located at nodes x_j . Notice that first-order approximations of the forward divided difference u^+ and the backward divided difference u^- at node x_j are $u_j^+ = u^+(x_j) = z_{j+\frac{1}{2}}$ and $u_j^- = u^-(x_j) = z_{j-\frac{1}{2}}$, respectively.

Next we introduce the following notations for the differences:

$$d_j = z_{j+\frac{1}{2}} - z_{j-\frac{1}{2}}, \quad (2.4)$$

$$d_{j+\frac{1}{2}} = \frac{d_j + d_{j+1}}{2}, \quad (2.5)$$

$$D_{j+\frac{1}{2}} = d_{j+1} - d_j. \quad (2.6)$$

The Weighted Power-ENO reconstruction is based on a convex combination of the following three candidate parabolas associated with each interval $I_j = [x_j, x_{j+1}]$:

$$p_j^P(x) = z_{j+\frac{1}{2}} - \frac{P_j}{24} + \frac{x - x_{j+\frac{1}{2}}}{\Delta x} \left[d_j + \frac{P_j}{2} + \frac{P_j}{2} \left(\frac{x - x_{j+\frac{1}{2}}}{\Delta x} \right) \right], \quad (2.7)$$

Power-ENO Schemes for Hamilton-Jacobi Equations

$$p_{j+\frac{1}{2}}(x) = z_{j+\frac{1}{2}} - \frac{D_{j+\frac{1}{2}}}{24} + \frac{x - x_{j+\frac{1}{2}}}{\Delta x} \left[d_{j+\frac{1}{2}} + \frac{D_{j+\frac{1}{2}}}{2} \left(\frac{x - x_{j+\frac{1}{2}}}{\Delta x} \right) \right], \quad (2.8)$$

$$p_{j+1}^P(x) = z_{j+\frac{1}{2}} - \frac{P_{j+1}}{24} + \frac{x - x_{j+\frac{1}{2}}}{\Delta x} \left[d_{j+1} - \frac{P_{j+1}}{2} + \frac{P_{j+1}}{2} \left(\frac{x - x_{j+\frac{1}{2}}}{\Delta x} \right) \right], \quad (2.9)$$

where

$$P_j := \text{powermod}_p(D_{j-\frac{1}{2}}, D_{j+\frac{1}{2}})$$

and

$$\text{powermod}_p(x, y) = \frac{(\text{sign}(x) + \text{sign}(y))}{2} \text{power}_p(|x|, |y|).$$

In particular, at $x = x_j$ we have

$$p_j^P(x_j) = z_{j+\frac{1}{2}} - \frac{1}{2}d_j - \frac{1}{6}P_j, \quad (2.10)$$

$$p_{j+\frac{1}{2}}(x_j) = z_{j+\frac{1}{2}} - \frac{1}{2}d_{j+\frac{1}{2}} - \frac{1}{6}D_{j+\frac{1}{2}}, \quad (2.11)$$

$$p_{j+1}^P(x_j) = z_{j+\frac{1}{2}} - \frac{1}{2}d_{j+1} + \frac{1}{3}P_{j+1}. \quad (2.12)$$

To obtain an optimal accuracy for $u^+(x_j)$ at the left interface of I_j we use the convex combination,

$$u^+(x_j) = w_0 \cdot p_j^P(x_j) + w_1 \cdot p_{j+\frac{1}{2}}(x_j) + w_2 \cdot p_{j+1}^P(x_j), \quad (2.13)$$

where

$$w_k = \frac{\alpha_k}{\alpha_0 + \alpha_1 + \alpha_2} \quad (2.14)$$

and

$$\alpha_k = \frac{C_k}{(\epsilon + IS_k)^2} \quad (2.15)$$

for $k = 0, 1, 2$. Here $C_0 = 0.6$, $C_1 = 0.2$, and $C_2 = 0.2$ are the optimal weights, and the smoothness indicators are

$$IS_0 = \frac{13}{12} (P_j)^2 + \frac{1}{4} \left(2z_{j+\frac{1}{2}} - 2z_{j-\frac{1}{2}} + P_j \right)^2, \quad (2.16)$$

$$IS_1 = \frac{13}{12} \left(z_{j-\frac{1}{2}} - 2z_{j+\frac{1}{2}} + z_{j+\frac{3}{2}} \right)^2 + \frac{1}{4} \left(z_{j-\frac{1}{2}} - z_{j+\frac{3}{2}} \right)^2, \quad (2.17)$$

$$IS_2 = \frac{13}{12} (P_{j+1})^2 + \frac{1}{4} \left(2z_{j+\frac{3}{2}} - 2z_{j+\frac{1}{2}} - P_{j+1} \right)^2, \quad (2.18)$$

where we have used the L^2 -norm of the derivatives of the corresponding polynomials to describe the smoothness so that the optimal order of accuracy can be achieved [15].

A similar formula for $u^-(x_j)$ is obtained from the polynomials associated with I_{j-1} ,

$$u^-(x_j) = w_0 \cdot p_{j-1}^P(x_j) + w_1 \cdot p_{j-\frac{1}{2}}(x_j) + w_2 \cdot p_j^P(x_j) \quad (2.19)$$

with $C_0=0.2$, $C_1=0.2$, and $C_2=0.6$ taken as the optimal weights in the formulas (2.14) and (2.15). Here the three parabolas evaluated at the right interface of I_{j-1} are,

$$p_{j-1}^P(x_j) = z_{j-\frac{1}{2}} + \frac{1}{2}d_{j-1} + \frac{1}{3}P_{j-1}, \quad (2.20)$$

$$p_{j-\frac{1}{2}}(x_j) = z_{j-\frac{1}{2}} + \frac{1}{2}d_{j-\frac{1}{2}} + \frac{1}{12}D_{j-\frac{1}{2}}, \quad (2.21)$$

$$p_j^P(x_j) = z_{j-\frac{1}{2}} + \frac{1}{2}d_j - \frac{1}{6}P_j. \quad (2.22)$$

The resulting reconstruction is a fifth-order accurate Weighted Power-ENO reconstruction for $p \geq 3$ as shown in [22]. The optimal value of p to get fifth-order accuracy for the approximation of hyperbolic conservation laws is $p=3$ as shown in [22]. In the following by the Weighted Power₃ENO5 scheme we mean $p=3$.

In addition, we are able to design a new scheme specifically for HJ equations with convex Hamiltonians. To this end we use the weakest possible limiter in the power limiter class, that is, the Power _{∞} mean, to define the Weighted Power _{∞} ENO5 reconstruction. In this case, simplified expressions for the three parabolas in terms of z_j 's are obtained at the right interface of I_{j-1} :

$$\begin{aligned} p_{j-1}^P(x_j) &= \frac{1}{6}z_{j-\frac{5}{2}} - \frac{2}{3}z_{j-\frac{3}{2}} + \frac{4}{3}z_{j-\frac{1}{2}} + \frac{1}{6}z_{j+\frac{1}{2}}, \\ p_{j-\frac{1}{2}}(x_j) &= -\frac{1}{6}z_{j-\frac{3}{2}} + \frac{5}{6}z_{j-\frac{1}{2}} + \frac{1}{3}z_{j+\frac{1}{2}}, \\ p_j^P(x_j) &= -\frac{1}{12}z_{j-\frac{3}{2}} + \frac{7}{12}z_{j-\frac{1}{2}} + \frac{7}{12}z_{j+\frac{1}{2}} - \frac{1}{12}z_{j+\frac{3}{2}}. \end{aligned}$$

Therefore, the corresponding smoothness indicators are,

$$\begin{aligned}
 IS_0 &= \frac{13}{48} \left(z_{j-\frac{5}{2}} - z_{j-\frac{3}{2}} - z_{j-\frac{1}{2}} + z_{j+\frac{1}{2}} \right)^2 \\
 &\quad + \frac{1}{4} \left(\frac{1}{2} z_{j-\frac{5}{2}} - \frac{5}{2} z_{j-\frac{3}{2}} + \frac{3}{2} z_{j-\frac{1}{2}} + \frac{1}{2} z_{j+\frac{1}{2}} \right)^2, \\
 IS_1 &= \frac{13}{12} \left(z_{j-\frac{1}{2}} - 2z_{j+\frac{1}{2}} + z_{j+\frac{3}{2}} \right)^2 + \frac{1}{4} \left(z_{j-\frac{1}{2}} - z_{j+\frac{3}{2}} \right)^2, \\
 IS_2 &= \frac{13}{48} \left(z_{j-\frac{3}{2}} - z_{j-\frac{1}{2}} - z_{j+\frac{1}{2}} + z_{j+\frac{3}{2}} \right)^2 \\
 &\quad + \frac{1}{4} \left(\frac{1}{2} z_{j-\frac{3}{2}} - \frac{5}{2} z_{j-\frac{1}{2}} + \frac{3}{2} z_{j+\frac{1}{2}} + \frac{1}{2} z_{j+\frac{3}{2}} \right)^2.
 \end{aligned}$$

Accordingly we can compute $u^-(x_j)$. Similarly we can derive the formula for computing $u^+(x_j)$.

Remark 1. The Weighted Power₃ENO5 reconstruction proposed in [22] is fifth-order accurate and is suitable for the approximation of hyperbolic conservation laws, since it satisfies the “local total variation bounded (LTVB)” property, as shown in [22]. This property is important for a reconstruction procedure to approximate piecewise smooth functions with jump discontinuities.

Remark 2. A limiter is designed to ignore the non-smooth information of solutions so that the total variation at jump discontinuities is diminished. However, when the solution is smooth in some region, the limiter also ignores smooth information from neighboring cells such that the loss of accuracy occurs in such smooth regions. Such a drawback is shared by both the WENO5 reconstruction and the WPower₃ENO5 reconstruction since the coefficients of the convex combination for the three different parabolas may change abruptly, and the resulting reconstruction degenerates to third-order accuracy.

Remark 3. From the one dimensional HJ equation

$$\phi_t + H(\phi_x) = 0, \tag{2.23}$$

$$\phi(x, 0) = \phi_0(x), \tag{2.24}$$

where H is convex, we can derive a corresponding hyperbolic conservation law by differentiating the equation once with respect to the spatial variable x ,

$$u_t + H_x(u) = 0, \quad (2.25)$$

$$u(x, 0) = \phi'_0(x), \quad (2.26)$$

where $u = \frac{\partial}{\partial x}\phi$. Then, by Corrias *et al.* [7] and Jin and Xin [16] ϕ is the viscosity solution of the convex HJ equation (2.23), (2.24) if and only if $u = \frac{\partial}{\partial x}\phi$ is the entropy solution of the convex hyperbolic conservation law (2.25), (2.26). According to our computational experience, the Weighted Power $_{\infty}$ ENO5 works for non-linear convex scalar hyperbolic conservation laws, but it has overshoots and undershoots around shocks since it lacks the LTVB property [22] and is overcompressive. However, for non-linear convex HJ equations we have found that the Weighted Power $_{\infty}$ ENO5 reconstruction works very well in practice as shown in the examples. Although a rigorous justification for this is still lacking, a possible explanation is that the overshoots and undershoots at shocks occurred in the entropy solution for a convex hyperbolic conservation law will be averaged once integrated, and such an integration step yields exactly the viscosity solution for the corresponding convex HJ equation (see Example 1 in Sec. 3). On the other hand, when the Hamiltonian is non-convex, the over-compressive Weighted Power $_{\infty}$ ENO5 reconstruction may give rise to numerical approximations that converge to other generalized solutions rather than the viscosity solution.

Remark 4. Because the reconstruction procedure for multi-dimensional HJ equations is done dimension-by-dimension, we can apply the above procedure in each direction to obtain high-order approximations to spatial derivatives to be used in numerical Hamiltonians.

2.2. Monotone Numerical Hamiltonians

Since most of our numerical examples are two-dimensional, in this section, we restrict our discussion to the two-dimensional case of Eq. (1.1):

$$\phi_t + H(\phi_x, \phi_y) = 0, \quad \phi(x, y, 0) = \phi_0(x, y), \quad t > 0. \quad (2.27)$$

The more general case can be treated similarly.

Let $\{(x_j, y_k, t^n)\}$ be a uniform discretization of $\mathcal{R}^2 \times [0, T]$ with mesh sizes Δx , Δy and Δt . $\phi_{j,k}^n$ denotes a numerical approximation to the viscosity solution of Eq. (2.27) at a generic point (x_j, y_k, t^n) ,

$$\phi(x_j, y_k, t^n) = \phi(j\Delta x, k\Delta y, n\Delta t). \quad (2.28)$$

We consider a first-order forward Euler scheme,

$$\phi_{j,k}^{n+1} = \phi_{j,k}^n - \Delta t g \left(\frac{\Delta_x^- \phi_{j,k}^n}{\Delta x}, \frac{\Delta_x^+ \phi_{j,k}^n}{\Delta x}, \frac{\Delta_y^- \phi_{j,k}^n}{\Delta y}, \frac{\Delta_y^+ \phi_{j,k}^n}{\Delta y} \right), \quad (2.29)$$

where g is a Lipschitz continuous, consistent and monotone numerical Hamiltonian. Here consistency of g means that $g(u, u, v, v) = H(u, v)$, and monotonicity means that g is non-increasing in its second and fourth arguments and non-decreasing in the other two. In addition, we used standard notations to denote forward and backward differences:

$$\Delta_x^- \phi_{j,k}^n = \phi_{j,k}^n - \phi_{j-1,k}^n, \quad \Delta_x^+ \phi_{j,k}^n = \phi_{j+1,k}^n - \phi_{j,k}^n; \quad (2.30)$$

$$\Delta_y^- \phi_{j,k}^n = \phi_{j,k}^n - \phi_{j,k-1}^n, \quad \Delta_y^+ \phi_{j,k}^n = \phi_{j,k+1}^n - \phi_{j,k}^n. \quad (2.31)$$

We may choose different monotone numerical Hamiltonians as the basis for first-order schemes [19, 20]. The following monotone numerical Hamiltonians are used in the numerical examples shown below.

The Lax-Friedrichs numerical Hamiltonian is [20]:

$$g^{LF}(u^-, u^+, v^-, v^+) = H \left(\frac{u^- + u^+}{2}, \frac{v^- + v^+}{2} \right) - \frac{1}{2} \alpha_1 (u^+ - u^-) - \frac{1}{2} \alpha_2 (v^+ - v^-),$$

where, for $a \leq u \leq b$ and $c \leq v \leq d$, $\alpha_1 = \max |H_1(u, v)|$ and $\alpha_2 = \max |H_2(u, v)|$, $H_j(u, v)$ being the partial derivative of H with respect to its j th argument, u^\pm and v^\pm being first-order forward and backward divided differences of ϕ in x and y directions, respectively.

The Godunov numerical Hamiltonian is [20]:

$$g^{G1}(u^-, u^+, v^-, v^+) = \text{ext}_{v \in I(v^-, v^+)} \text{ext}_{u \in I(u^-, u^+)} H(u, v),$$

where $I(a, b) = [\min(a, b), \max(a, b)]$, and

$$\text{ext}_{u \in I(a, b)} = \begin{cases} \min_{a \leq u \leq b} & a \leq b, \\ \min_{b \leq u \leq a} & a > b. \end{cases}$$

When $H(u, v) = h(u^2, v^2)$, such that $h_1 \cdot h_2 > 0$, where h_j is the partial derivative of h with respect to its j th argument, we use the Osher–Sethian numerical Hamiltonian [19]:

$$g^{G2}(u^-, u^+, v^-, v^+) = \begin{cases} h([\max((u^-)^+, (u^+)^-)]^2, [\max((v^-)^+, (v^+)^-)]^2) & h_1 \geq 0, \\ h([\max((u^-)^-, (u^+)^+)]^2, [\max((v^-)^-, (v^+)^+)]^2) & \text{otherwise,} \end{cases}$$

where $(a)^+ = \max(a, 0)$ and $(a)^- = -\min(a, 0)$.

In summary, to obtain higher order finite difference schemes for HJ equations, the strategy is to first approximate spatial derivatives u^\pm and v^\pm with higher order finite differences, such as WENO5, Weighted Power₃ENO5 or Weighted Power_∞ENO5 reconstructions, then insert them into monotone Hamiltonians, and finally use higher order SSP-RK time stepping to march in time [23, 25]. This completes our construction for Weighted Power-ENO schemes.

3. NUMERICAL EXPERIMENTS

3.1. Example 1

Given the hyperbolic conservation law (CL),

$$u_t + \left(\frac{u^2}{2}\right)_x = 0 \quad (3.1)$$

with the initial data,

$$u(x, 0) = \begin{cases} -1, & x < 0; \\ 1, & 0 \leq x \leq 4; \\ -1, & x > 4, \end{cases}$$

we can obtain a HJ equation

$$\phi_t + \frac{\phi_x^2}{2} = 0 \quad (3.2)$$

with the initial data

$$\phi(x, 0) = \begin{cases} -x - 5, & x < 0; \\ x - 5, & 0 \leq x \leq 4; \\ -x + 3, & x > 4 \end{cases}$$

by introducing $\phi(x, t) = \int_{-5}^x u(s, t) ds$.

We compute the approximate solutions at $t = 4$ for the HJ equation using two procedures:

- (1) integrating the HJ equation directly by the Weighted Power_∞ ENO5 scheme;
- (2) computing the primitive of the numerical solution of the CL with the constant of integration $\phi(-5, 4) = -2$, where the numerical solution is computed by the Weighted Power_∞ENO5: if u_j^n is

Power-ENO Schemes for Hamilton-Jacobi Equations

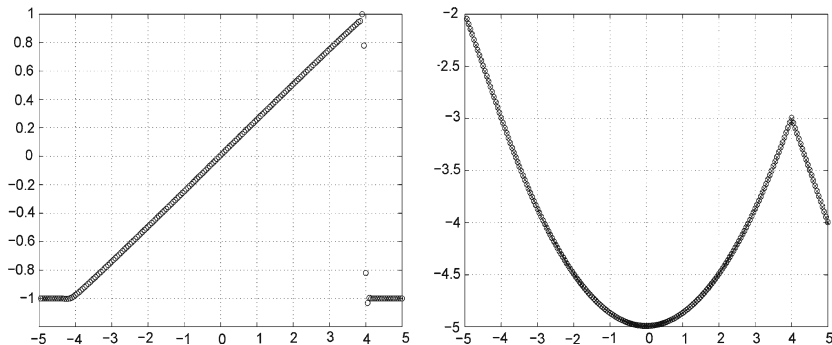


Fig. 1. Left: numerical solution by the $\text{WPower}_\infty\text{ENO5}$ for the conservation law. Right: numerical solution by the $\text{WPower}_\infty\text{ENO5}$ for the HJ equation ('+') versus integration of numerical solution by the $\text{WPower}_\infty\text{ENO5}$ for the CL equation ('o').

the solution to the CL, then

$$\phi_j^n = -2 + \frac{h}{2}u_1 + \sum_{i=2}^{j-1} \Delta x \cdot u_i + \frac{h}{2}u_j. \quad (3.3)$$

Figure 1 illustrates the results. The left sub-figure shows the approximation to the CL by the $\text{WPower}_\infty\text{ENO5}$, in which we observe the overshoot and the undershoot due to the over-compressive property of the Weighted $\text{Power}_\infty\text{ENO5}$ reconstruction around discontinuities. The right sub-figure displays the solutions obtained by the above two procedures, and they match with each other very nicely. In particular, we note that the numerical integration procedures cancel out the over-compressive effect on discontinuities.

Next, we apply the Weighted $\text{Power}_3\text{ENO5}$ scheme and the Weighted $\text{Power}_\infty\text{ENO5}$ scheme to a set of model problems. Along the way we compare our schemes with the standard WENO5 scheme to justify our numerical results.

3.2. Example 2

(One dimension). We consider

$$\phi_t + H(\phi_x) = 0, \quad -1 \leq x \leq 1, \quad t > 0, \quad (3.4)$$

$$\phi(x, 0) = -\cos(\pi x), \quad -1 \leq x \leq 1 \quad (3.5)$$

with a convex Hamiltonian, $H(u) = \frac{(u+1)^2}{2}$, and a non-convex Hamiltonian, $H(u) = -\cos(u+1)$.

We solve both initial value problems up to two different times $t=t_1=0.05$ and $t=t_2=0.16$. The solution is smooth up to $t=t_1$, and its derivative is discontinuous at $t=t_2$ in both cases. For the convex case, we use WENO5, Weighted Power₃ENO5, and Weighted Power_∞ENO5 schemes; for the non-convex case, we use WENO5 and Weighted Power₃ENO5 schemes only. The numerical Hamiltonian is chosen to be g^{G1} .

In Tables I–IV, we display the L_∞ and L_1 errors in different cases. At $t=t_2$ the errors are computed at a distance 0.1 away from discontinuities in the derivative of the solution. For time stepping in the three schemes, we have used the third-order SSP-RK scheme [20] by taking $\Delta t \approx \Delta x^{5/3}$ to realize fifth-order in time.

For the convex case, at t_1 the smallest L_∞ -error is reached by the Weighted Power_∞ENO5 scheme since the local truncation error in its reconstruction is the smallest among all Weighted Power-ENO reconstructions [22]; at t_2 this scheme has the largest L_∞ -errors (due to the presence of discontinuities) among the three schemes. We notice that the fifth-order accuracy in smooth regions is achieved in all the cases.

3.3. Example 3

(Two dimensions). We solve

$$\phi_t + H(\phi_x, \phi_y) = 0, \quad -2 \leq x, \quad y \leq 2, \quad t > 0, \quad (3.6)$$

$$\phi(x, 0) = -\cos \pi \left(\frac{x+y}{2} \right), \quad -2 \leq x, \quad y \leq 2 \quad (3.7)$$

with a convex Hamiltonian, $H(u) = \frac{(u+v+1)^2}{2}$. We compute the solution up to $t=0.05$ by the three schemes with the numerical Hamiltonian being g^{G1} .

Table I. $H(u) = \frac{(u+1)^2}{2}$ at $t=0.05$

Scheme	N	L_∞ error	L_∞ order	L_1 error	L_1 order
WENO5-GODUNOV	40	0.16E-04	–	0.50E-04	–
	80	0.76E-06	4.45	0.21E-05	4.59
	160	0.30E-07	4.66	0.88E-07	4.55
WPower ₃ ENO5-GODUNOV	40	0.56E-04	–	0.76E-04	–
	80	0.20E-05	4.81	0.29E-05	4.70
	160	0.73E-07	4.77	0.11E-06	4.75
WPower _∞ ENO5-GODUNOV	40	0.53E-05	–	0.15E-04	–
	80	0.20E-06	4.71	0.60E-06	4.61
	160	0.96E-08	4.39	0.25E-07	4.63

Power-ENO Schemes for Hamilton-Jacobi Equations

Table II. $H(u) = \frac{(u+1)^2}{2}$ at $t=0.16$

Scheme	N	L_∞ error	L_∞ order	L_1 error	L_1 order
WENO5-GODUNOV	40	0.31E-03	–	0.38E-03	–
	80	0.86E-05	5.17	0.13E-04	4.87
	160	0.14E-06	5.87	0.26E-06	5.60
	320	0.47E-08	4.96	0.69E-08	5.28
WPower ₃ ENO5-GODUNOV	40	0.17E-03	–	0.37E-03	–
	80	0.13E-04	3.68	0.25E-04	3.88
	160	0.21E-06	6.04	0.46E-06	5.76
	320	0.22E-08	6.55	0.61E-08	6.24
WPower _∞ ENO5-GODUNOV	40	0.25E-02	–	0.50E-02	–
	80	0.44E-03	2.52	0.52E-03	3.26
	160	0.24E-04	4.20	0.24E-04	4.41
	320	0.42E-06	5.86	0.43E-06	5.84

Table III. $H(u) = -\cos(u+1)$ at $t=0.05$

Scheme	N	L_∞ error	L_∞ order	L_1 error	L_1 order
WENO5-GODUNOV	40	0.47E-04	–	0.13E-03	–
	80	0.31E-05	3.89	0.65E-05	4.28
	160	0.14E-06	4.52	0.27E-06	4.60
	40	0.67E-04	–	0.15E-03	–
WPower ₃ ENO5-GODUNOV	80	0.84E-05	3.05	0.13E-04	3.48
	160	0.73E-06	3.53	0.10E-05	3.73

Table IV. $H(u) = -\cos(u+1)$ at $t=0.16$

Scheme	N	L_∞ error	L_∞ order	L_1 error	L_1 order
WENO5-GODUNOV	40	0.16E-03	–	0.31E-03	–
	80	0.15E-04	3.41	0.31E-04	3.29
	160	0.71E-06	4.43	0.12E-05	4.76
	320	0.21E-07	5.07	0.35E-07	5.04
WPower ₃ ENO5-GODUNOV	40	0.12E-03	–	0.28E-03	–
	80	0.11E-04	3.43	0.19E-04	3.88
	160	0.12E-05	3.13	0.13E-05	3.89
	320	0.22E-07	5.78	0.32E-07	5.33

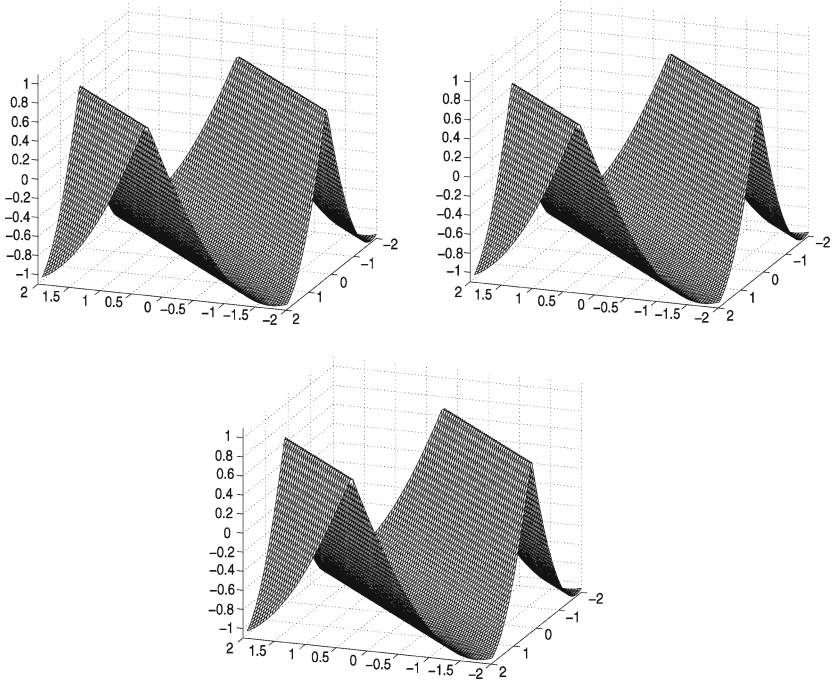


Fig. 2. Top left, WENO5. Top right, WPower₃ENO5. Bottom, WPower_∞ENO5. Mesh: 80×80 .

Figure 2 shows that the computed solutions by the three schemes on 80×80 meshes converge to the viscosity solution.

Figure 3 presents the calibration results for some chosen slices of the two-dimensional solutions on different meshes; in particular, we notice that the Weighted Power₃ENO5 scheme has sharper resolution near kinks than the classical WENO5 scheme does; in turn, the WPower_∞ENO5 scheme has sharper resolution near kinks than the Weighted Power₃ENO5 scheme does.

3.4. Example 4

We solve the linear equation

$$\phi_t + \phi_x = 0, \quad (3.8)$$

$$\phi(x, 0) = f(x - 0.5), \quad -1 \leq x \leq 1 \quad (3.9)$$

with periodic boundary conditions.

Power-ENO Schemes for Hamilton-Jacobi Equations

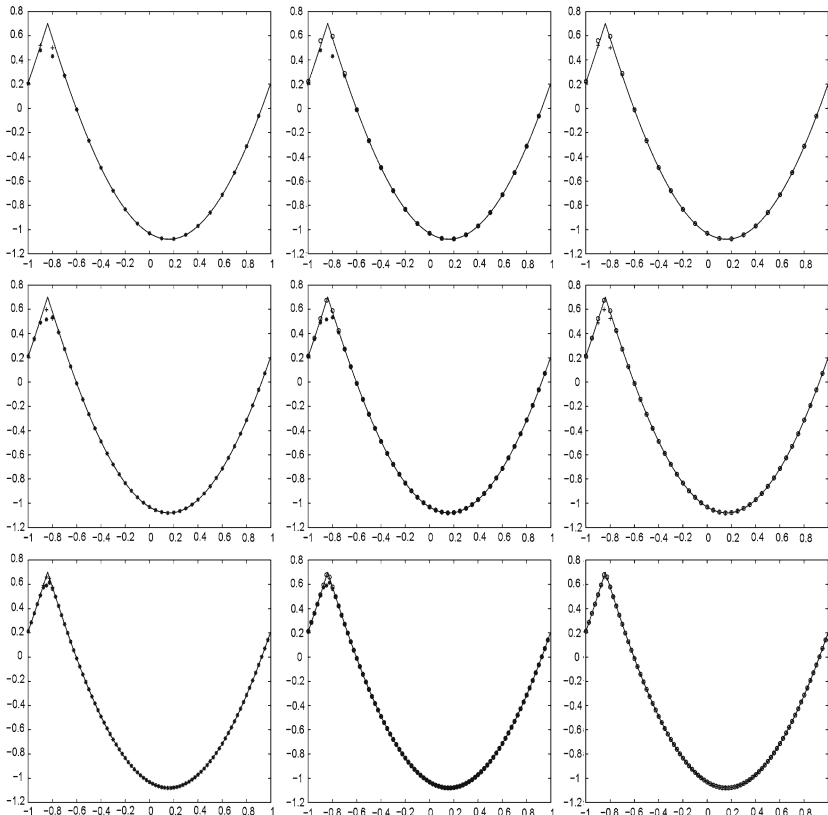


Fig. 3. Comparisons. Left column: WENO5 ('*') and WPower₃ENO5 ('+'). Central column: WENO5 ('*') and WPower_∞ENO5 ('o'). Right column: Weighted Power₃ENO5 ('+') and WPower_∞ENO5 ('o') with 20, 40, and 80 points.

We choose $f(x)$ to be a primitive of the Harten function which is discontinuous [12]:

$$f(x) = -\left(\frac{\sqrt{3}}{2} + \frac{9}{2} + \frac{2\pi}{3}\right)(x+1) + \begin{cases} 2 \cos\left(\frac{3\pi x^2}{2}\right) - \sqrt{3}, & -1 \leq x \leq -\frac{1}{3}; \\ 3/2 + 3 \cos(2\pi x), & -\frac{1}{3} \leq x \leq 0; \\ 15/2 - 3 \cos(2\pi x), & 0 \leq x \leq \frac{1}{3}; \\ (28 + 4\pi + \cos(3\pi x))/3 + 6\pi(x^2 - x), & \frac{1}{3} \leq x \leq 1. \end{cases}$$

The results computed with 100 grid points and CFL=0.6 at times $t = 2, 8, 16$ and 32 are shown in Fig. 4. We observe that as time increases all schemes smooth out the corners. However, both Weighted Power₃ENO5 and Weighted Power_∞ENO5 schemes perform better than the classical

WENO5 scheme at the kinks in terms of capturing sharp transitions. Moreover, the plots also indicate that the Weighted Power $_{\infty}$ ENO5 scheme outperforms the other two at those kinks.

3.5. Example 5

We solve a two-dimensional non-convex Riemann problem,

$$\phi_t + \sin(\phi_x + \phi_y) = 0, \quad \phi(x, y, 0) = \pi(|y| - |x|). \quad (3.10)$$

We evolve up to time $t=1$ with a grid of 40×40 points using the WENO and Weighted Power $_3$ ENO5 schemes based on the numerical Hamiltonian g^{G1} .

The solutions by the two schemes converge to the viscosity solution as shown in Fig. 5.

3.6. Example 6

We consider a problem related to optimal control [20]:

$$\phi_t - (\sin y)\phi_x + (\sin x + \text{sign}(\phi_y))\phi_y - \frac{1}{2}\sin^2 y - (1 - \cos x) = 0 \quad (3.11)$$

with the initial data $\phi(x, y, 0) = 0$ in the interval $[-\pi, \pi] \times [-\pi, \pi]$. We use a grid of 40×40 with periodic boundary conditions.

We compute the solution up to $t=1$ by using WENO5, WPower $_3$ ENO5, and WPower $_{\infty}$ ENO5 schemes based on the Lax-Friedrichs numerical Hamiltonian and the third-order SSP-RK scheme. We display the results at $t=1$ in Fig. 6.

3.7. Example 7

Consider the “level set reinitialization” equation

$$\phi_t + \text{sign}(\phi_0) \left[\sqrt{\phi_x^2 + \phi_y^2} - 1 \right] = 0, \quad \phi(x, y, 0) = \phi_0(x, y). \quad (3.12)$$

We solve this equation using WENO5, WPower $_3$ ENO5, and WPower $_{\infty}$ ENO5 schemes. We choose ϕ_0 to be the signed distance function to the circle centered at the origin with radius $1/2$; in addition, some perturbation is added to the signed distance function in radial and angular directions near the circle. In particular, we use two different initial conditions with different amounts of perturbation to illustrate the robustness of the

Power-ENO Schemes for Hamilton-Jacobi Equations

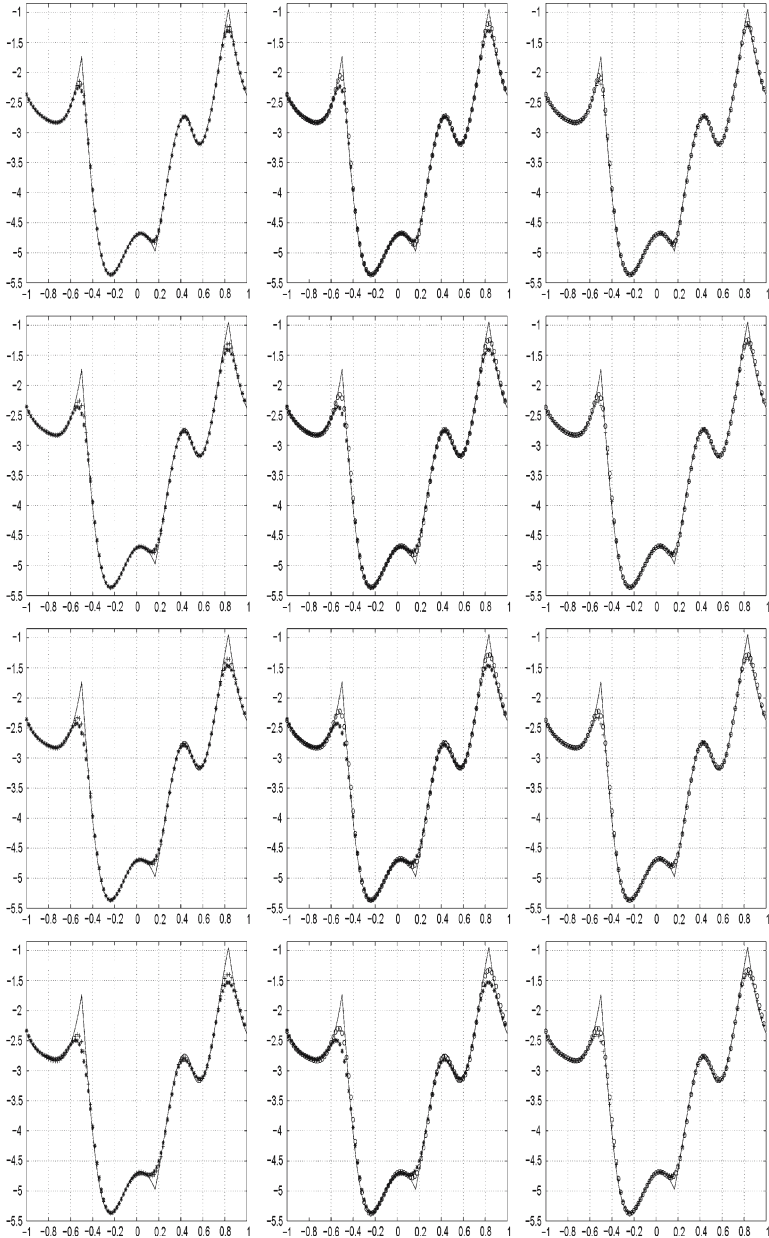


Fig. 4. Comparisons. Left column: WENO5 ('*') and WPower₃ENO5 ('+'). Central column: WENO5 ('*') and WPower_∞ENO5 ('o'). Right column: WPower₃ENO5 ('+') and WPower_∞ENO5 ('o') at time 2, 8, 16, and 32 from top to bottom.

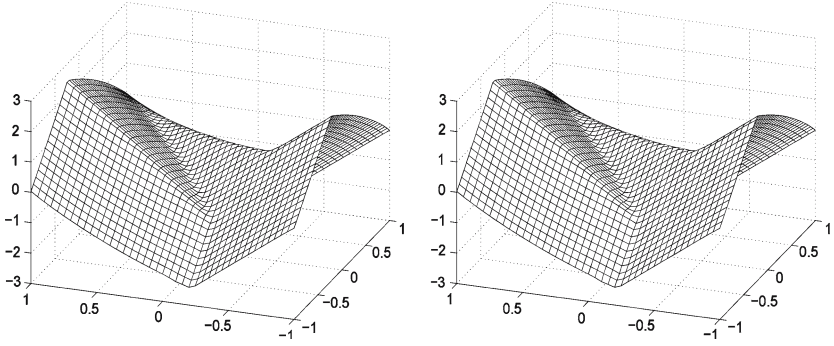


Fig. 5. Left: WENO5. Right: WPower₃ENO5.

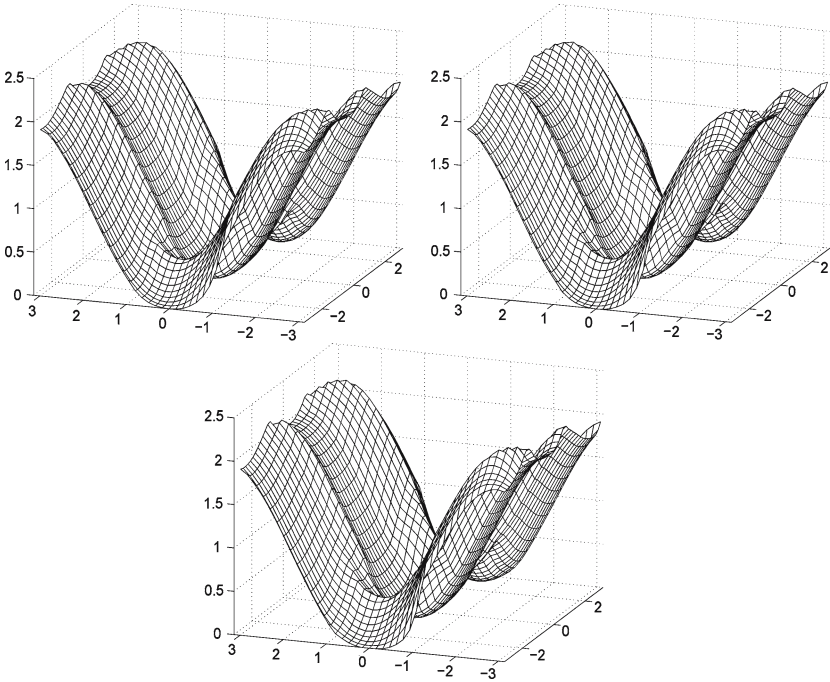


Fig. 6. Top left, WENO5. Top right, WPower₃ENO5. Bottom, WPower_∞ENO5.

WPower_∞ENO5 scheme. Here,

$$\phi_0^1(x, y) = \begin{cases} d + \delta, & |d| \leq \epsilon, \\ d, & \text{otherwise,} \end{cases} \quad (3.13)$$

$$\phi_0^2(x, y) = \begin{cases} d + 2\delta, & |d| \leq \epsilon, \\ d, & \text{otherwise,} \end{cases} \quad (3.14)$$

where $d = \sqrt{x^2 + y^2} - 0.5$, $\theta = \tan^{-1}(\frac{y}{|x|})$, $\epsilon = 0.2$, and $\delta = \frac{\epsilon}{16\pi} \sin\left(\frac{4\pi d \sin 5\theta}{\epsilon}\right)$.

We use $\frac{\phi_0}{\sqrt{\phi_0 + (\Delta x)^2}}$ to approximate $\text{sign}(\phi_0)$.

We perform the computation using the Osher–Sethian flux g^{G_2} , which is simpler than the general one, g^{G_1} , together with the third-order SSP-RK time stepping for the three schemes. We evolve in time using a grid of 100×100 points and a CFL number of 0.6.

At different times we compute the mean curvature, $K \equiv \nabla \cdot \frac{\nabla \phi}{|\nabla \phi|}$, of the level set contours, by using central differences. As a regularization for the possible zero denominator, we replace $\frac{\nabla \phi}{|\nabla \phi|}$ with $\frac{\nabla \phi}{\sqrt{|\nabla \phi|^2 + \Delta x^2}}$.

For the first case corresponding to ϕ_0^1 , the maximum of the mean curvature of the initial data is 43.545925 and the minimum is -33.465937 ; for the second case corresponding to ϕ_0^2 , the maximum is 88.5558 and the minimum -66.4770 .

Figure 7 shows the results for the first case. From top to bottom we display the initial data and the results for steps 16, 64, and 256.

Figure 8 shows the results for the second case. From top to bottom we display the initial data and the results for steps 128, 512, and 1024.

In both cases there are significant differences in the curvature before and after the reinitialization. The curvature computed from the solution by the Weighted Power $_{\infty}$ ENO5 scheme is less noisy in both cases than both WENO5 and Weighted Power $_3$ ENO5 schemes; the noise persists in some regions for the latter two schemes. Although the behavior of WENO5 and Weighted Power $_3$ ENO5 schemes is similar, the noise dissipates for the Weighted Power $_{\infty}$ ENO5 scheme; we believe that the non-smooth limiters in the WENO5 and Weighted Power $_3$ ENO5 schemes might cause the persistence of some degree of noise in the curvature, and the arithmetic mean type limiter in the Weighted Power $_{\infty}$ ENO5 scheme might be responsible for the better behavior of the scheme.

Next, we consider the recovery of a non-smooth distance function. For this purpose, we choose ϕ_0 to be the signed distance function, $d_l(x, y)$, to the lemniscate,

$$a^4 = [(x - a)^2 + y^2][(x + a)^2 + y^2] \quad (3.15)$$

with $a = 0.5$, plus some perturbation in radial and angular directions near the curve:

$$\phi_0^3(x, y) = \begin{cases} d_l + 3\delta, & |d_l| \leq \epsilon, \\ d_l, & \text{otherwise,} \end{cases} \quad (3.16)$$

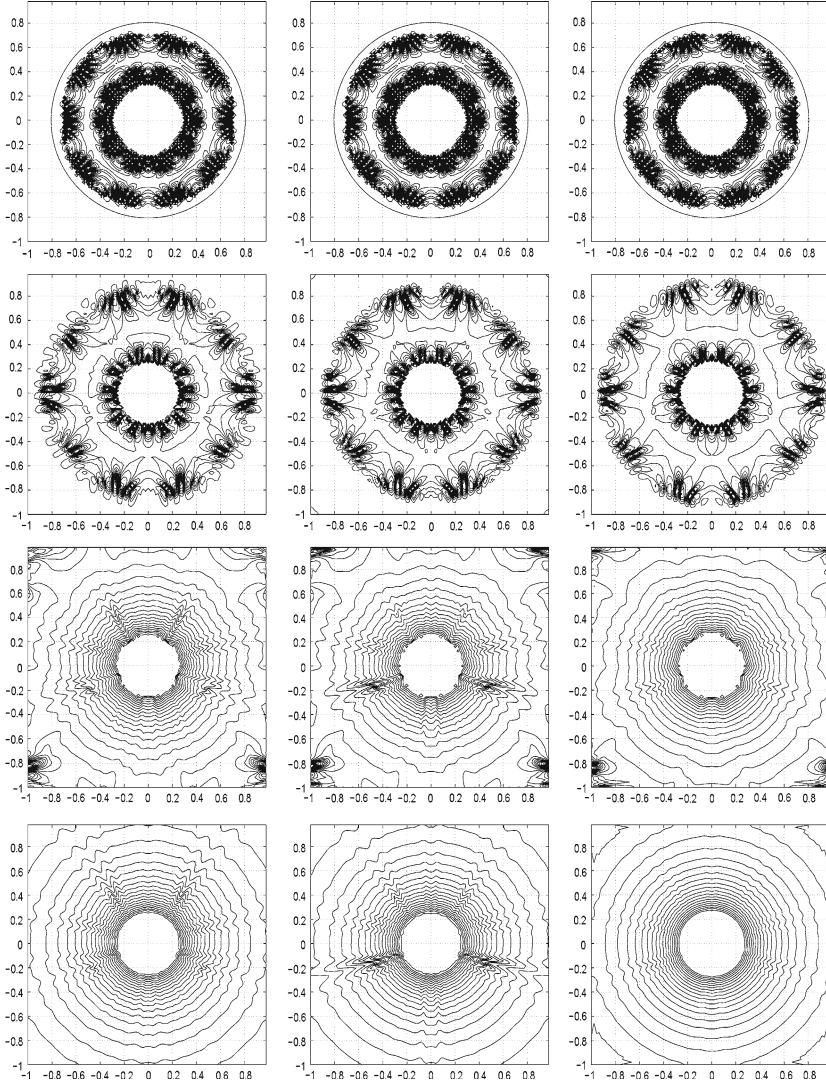


Fig. 7. ϕ_0^1 as the initial condition. Curvatures at steps 0, 16, 64, and 256. Left column: WENO5. Central column: WPower₃ENO5. Right column: Weighted Power_∞ENO5.

Power-ENO Schemes for Hamilton-Jacobi Equations

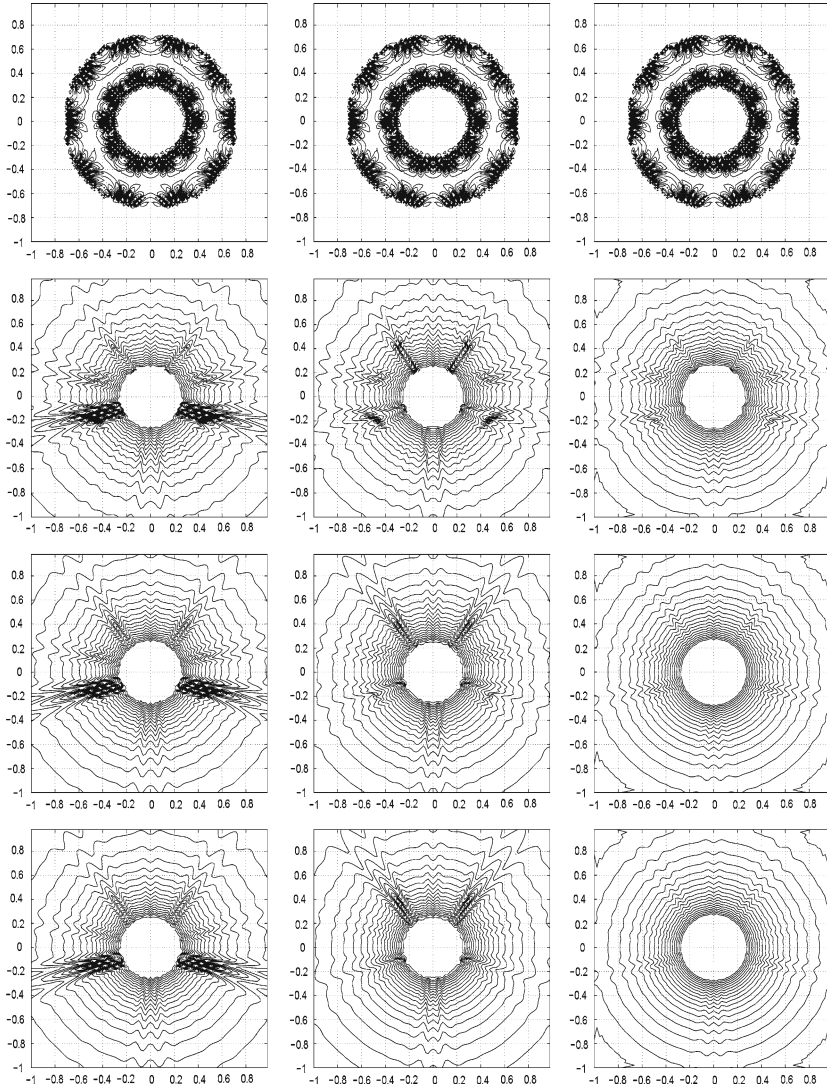


Fig. 8. ϕ_0^2 as the initial condition. Curvatures at steps 0, 128, 512 and 1024. Left column: WENO5. Central column: WPower₃ENO5. Right column: Weighted Power_∞ENO5.

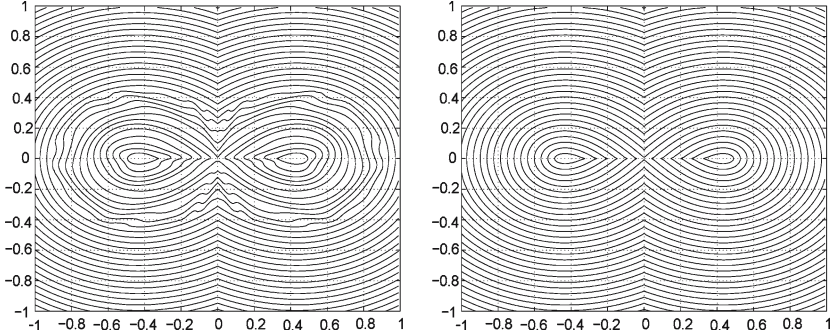


Fig. 9. Left: perturbed initial data. Right: converged solution by Weighted Power $_{\infty}$ ENO5.

which is defined in $[-1, 1] \times [-1, 1]$ with $\delta = \frac{\epsilon}{16\pi} \sin\left(\frac{2\pi d \sin 5\theta}{\epsilon}\right)$, $\epsilon = 0.2$ and $\theta = \tan^{-1}\left(\frac{y}{|x|}\right)$. Here we compute the signed distance function to the lemniscate by evolving through (3.12) to the steady state the following initial data:

$$D(x, y) = \sqrt{[(x-a)^2 + y^2][(x+a)^2 + y^2]} - a^2. \quad (3.17)$$

Let us remark that $d_l(x, y)$ has a jump discontinuity in first-order partial derivatives along the y -axis.

We evolve in time using a grid of 200×200 and a CFL number of 0.6 for the three schemes. At different times we compute the corresponding mean curvature of ϕ in the domain excluding small neighborhoods of the x - and y -axis so as to improve visualization of the noise in contour lines.

In Fig. 9, we display the initial perturbed data ϕ_0^3 and only the converged solution (to the steady state) by the Weighted Power $_{\infty}$ ENO scheme since there is no distinguishable difference in the steady state solutions by the three schemes.

Figure 10 shows the contour plots of the curvature. From top to bottom we display the initial data and the results for steps 16, 64, and 256.

We remark that the solutions by the three schemes converge to steady states very fast and a significant reduction of the noise in the computed curvatures is achieved in all cases.

Finally, we also remark that we have used the fourth-order SSP-RK time stepping procedure designed by Spiteri and Ruuth [25] in the computation; the main advantage of fourth-order SSP-RK is that we can speed up the computation 50% by doubling the CFL number to achieve the same accuracy.

Power-ENO Schemes for Hamilton-Jacobi Equations

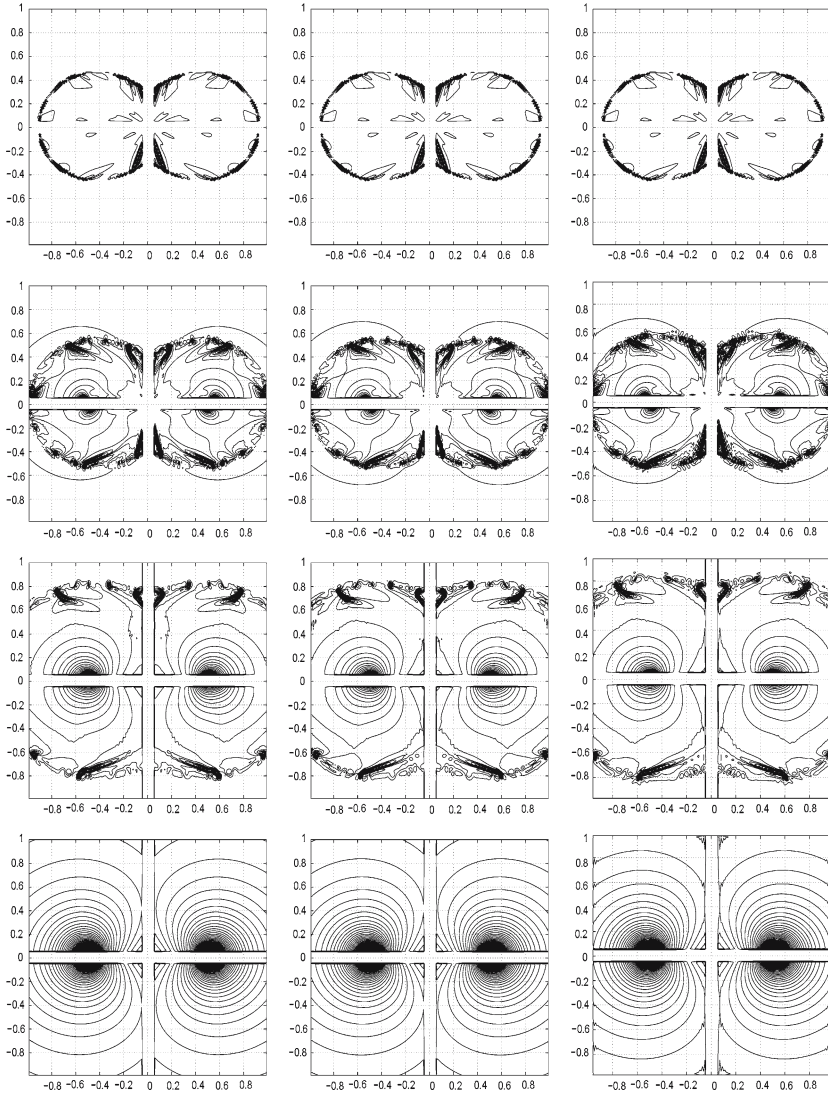


Fig. 10. Curvatures at steps 0, 16, 64, and 256. Left column: WENO5. Central column: WPower₃ENO5. Right column: Weighted Power_∞ENO5.

4. CONCLUSIONS

We have designed a class of Weighted Power-ENO schemes to approximate the viscosity solution of the HJ equations. The essential idea of the Power-ENO reconstruction is to apply a class of extended limiters to second-order differences in the classical third-order ENO reconstruction so as to improve resolution near discontinuities. Then a weighting strategy based on appropriate smoothness indicators lifts schemes to be fifth-order accurate. Numerical experiments have demonstrated the accuracy and the robustness of the new schemes.

ACKNOWLEDGMENTS

The authors would thank Prof. A. Marquina and Prof. S. Osher for discussions on this topic. The first author performed the research reported here while being a guest of the Department of Mathematics at UCLA; Serna thanks the computational and applied mathematics group members for their hospitality. Susana Serna Research supported by DGICYT projects BFM2001-2814 and MTM2005-07708. Jianliang Qian Research supported by ONR Grant #N00014-02-1-0720.

REFERENCES

1. Abgrall, R. (1996). Numerical discretization of the first-order Hamilton-Jacobi equations on triangular meshes. *Comm. Pure Appl. Math.* **49**, 1339–1377.
2. Albert, S., Cockburn, B., French, D., and Peterson, T. (2002). A posteriori error estimates for general numerical methods for Hamilton-Jacobi equations. Part I: the steady state case. *Math. Comp.* **71**, 49–76.
3. Bryson, S., and Levy, D. (2003). High-order central WENO schemes for multi-dimensional Hamilton-Jacobi equations. *SIAM J. Num. Anal.* **41**, 1339–1369.
4. Cecil, T., Qian, J., and Osher, S. J. (2004). Numerical methods for high dimensional Hamilton-Jacobi equations using radial basis functions. *J. Comp. Phys.* **196**, 327–347.
5. Cockburn, B., and Qian, J. (2002). Continuous dependence results for Hamilton-Jacobi equations. In Estep D. and Tavener S. *Collected Lectures on the Preservation of Stability Under Discretization*. SIAM, Philadelphia, PA, pp. 67–90.
6. Cockburn, B., and Yenikaya, B. (2005). An adaptive method with rigorous error control for the Hamilton-Jacobi equations. Part I: the one dimensional steady state case. *Appl. Numer. Math.* **52**, (2–3): 175–195.
7. Corrias, L., Falcone, M., and Natalini, R. (1995). Numerical schemes for conservation laws via Hamilton-Jacobi equations. *Math. Comp.* **64**, 555–580.
8. Crandall, M., and Lions, P. (1983). Viscosity solutions of Hamilton-Jacobi equations. *Trans. Am. Math. Soc.* **277**, 1–42.
9. Crandall, M., and Lions, P. (1984). Two approximations of solutions of Hamilton-Jacobi equations. *Math. Comput.* **43**, 1–19.
10. Falcone, M., and Ferretti, R. (1994). Discrete time high order schemes for viscosity solutions of Hamilton-Jacobi-Bellman equations. *Numer. Math.* **67**, 315–344.

Power-ENO Schemes for Hamilton-Jacobi Equations

11. Gottlieb, S., Shu, C.W., and Tadmor, E. (2001). Strong stability preserving high-order time discretization methods. *SIAM Rev.* **43**, 89–112.
12. Harten, A. (1983). High resolution schemes for hyperbolic conservation laws. *J. Comput. Phys.* **49**, 357–393.
13. Harten, A., Engquist, B., Osher, S., and Chakravarthy, S. (1987). Uniformly high-order accurate essentially non-oscillatory schemes III. *J. Comput. Phys.* **71**, 231–303.
14. Jiang, G.S., and Peng, D. (2000). Weighted ENO schemes for Hamilton-Jacobi equations. *SIAM J. Sci. Comput.* **21**, 2126–2143.
15. Jiang, G.S., and Shu, C.W. (1996). Efficient Implementation of weighted ENO schemes. *J. Comput. Phys.* **126**, 202–228.
16. Jin, S., and Xin, ZP. (1998). Numerical passage from systems of conservation laws to Hamilton-Jacobi Equations and relaxation schemes. *SIAM J. Numer. Anal.* **35**, 2385–2404.
17. Lin, C. T., and Tadmor, E. (2000). High-resolution non-oscillatory central schemes for Hamilton-Jacobi Equations. *SIAM J. Sci. Comput.* **21**, 2163–2186.
18. Liu, X-D., Osher, S.J., and Chan, T. (1994). Weighted essentially non-oscillatory schemes. *J. Comput. Phys.* **115**, 200–212.
19. Osher, S.J., and Sethian, J. (1988). Fronts propagating with curvature dependent speed: Algorithms based on Hamilton-Jacobi formulations. *J. Comput. Phys.* **79**, 12–49.
20. Osher, S.J., and Shu, C.W. (1991). High-order essentially non-oscillatory schemes for Hamilton-Jacobi equations. *SIAM J. Numer. Anal.* **28**, 907–922.
21. Qiu, J., and Shu, C. W. (2005). Hermite WENO schemes for Hamilton-Jacobi equations. *J. Comput. Phys.* **204**, 82–99.
22. Serna, S., and Marquina, A. (2004). Power ENO Methods: a fifth-order accurate Weighted Power ENO method. *J. Comput. Phys.* **194**, 632–658.
23. Shu, C. W., and Osher, S. J. (1989). Efficient implementation of essentially non-oscillatory shock capturing schemes II. *J. Comput. Phys.* **83**, 32–78.
24. Souganidis, P. E. (1985). Approximation schemes for viscosity solutions of Hamilton-Jacobi equations. *J. Diff. Eqn.* **59**, 1–43.
25. Spiteri, R. J., and Ruuth, S. J. (2002). A new class of optimal high order strong stability preserving time discretization methods. *SIAM J. Num. Anal.* **40**, 469–491.
26. Zhang, Y.T., and Shu, C.W. (2003). High-order WENO schemes for Hamilton-Jacobi equations on triangular meshes. *SIAM J. Sci. Comput.* **24**, 1005–1030.